Heliyon 9 (2023) e21253

Contents lists available at ScienceDirect

Heliyon

journal homepage: www.cell.com/heliyon

Quantitative assessment of Land use/land cover changes in a developing region using machine learning algorithms: A case study in the Kurdistan Region, Iraq

Abdulqadeer Rash [a,c,*], Yaseen Mustafa [b], Rahel Hamad [a,c]

[a] Dept. of Petroleum Geosciences, Faculty of Science, Soran University, 44008, Soran, Erbil, Iraq
[b] Dept. of Environmental Sciences, Faculty of Science, University of Zakho, Duhok, Iraq
[c] Soran Research Centre, Soran University, Soran, Erbil, Iraq

ARTICLE INFO

Keywords:
Supervised classification
Change detection
Socioeconomics
Remote sensing
Landsat imagery

ABSTRACT

The identification of land use/land cover (LULC) changes is important for monitoring, evaluating, and preserving natural resources. In the Kurdistan region, the utilization of remotely sensed data to assess the effectiveness of machine learning algorithms (MLAs) for LULC classification and change detection analysis has been limited. This study monitors and analyzes LULC changes in the study area from 1991 to 2021 using a quantitative approach with multi-temporal Landsat imagery. Five MLAs were applied: Support Vector Machine (SVM), Random Forest (RF), Artificial Neural Network (ANN), K-Nearest Neighbor (KNN), and Extreme Gradient Boosting (XGBoost). The results showed that the RF algorithm produced the most accurate maps of the three-decade study period, accompanied by a high kappa coefficient (0.93–0.97) compared with the SVM (0.91–0.95), ANN (0.91–0.96), KNN (0.92–0.96), and XGBoost (0.92–0.95) algorithms. Consequently, the RF classifier was implemented to categorize all obtainable satellite images. Socioeconomic changes throughout these transition periods were revealed by the change detection results. Rangeland and barren land areas decreased by 11.33 % (−402.03 km^2) and 6.68 % (−236.8 km^2), respectively. The transmission increases of 13.54 % (480.18 km^2), 3.43 % (151.74 km^2), and 0.71 % (25.22 km^2) occurred in agricultural land, forest, and built-up areas, respectively. The outcomes of this study contribute significantly to LULC monitoring in developing regions, guiding stakeholders to identify vulnerable areas for better land use planning and sustainable environmental protection.

1. Introduction

Climate change and human activities have significantly impacted the Earth's land use and composition. Understanding and categorizing land use changes is crucial for investigating environmental transformations across spatiotemporal scales [1,2]. Human economic and population growth, as well as the demand for limited natural resources, have influenced land use patterns at both local and global levels [3]. Human-induced environmental problems pose a threat to future ecological limits. As maintaining evolving land use trends is a global challenge, comprehensive investigations into changes in land use/land cover (LULC) are indispensable for

* Corresponding author. Dept. of Petroleum Geosciences, Faculty of Science, Soran University, 44008, Soran, Erbil, Iraq.
E-mail addresses: abdulqadeer.ahmed@soran.edu.iq (A. Rash), yaseen.mustafa@uoz.edu.krd (Y. Mustafa), rahel.hamad@soran.edu.iq (R. Hamad).

https://doi.org/10.1016/j.heliyon.2023.e21253
Received 7 August 2023; Received in revised form 13 October 2023; Accepted 18 October 2023
Available online 24 October 2023
2405-8440/© 2023 The Authors. Published by Elsevier Ltd. This is an open access article under the CC BY-NC-ND license (http://creativecommons.org/licenses/by-nc-nd/4.0/).

preserving the environment and its natural resources [4,5].

In terms of the function and physical covering of a pattern, land use and land cover are generally interrelated concepts [6]. Land use classifications involve human activities, such as residential areas, transportation, industrial use, and crop cultivation [7]. Land cover refers to the continuous natural characteristics of the Earth's surface, such as vegetation, rocks, soil, and water bodies [8,9]. LULC changes are dynamic processes that occur on biophysical surfaces over time and location [10]. These changes can be categorized as comprehensive replacements, such as rangeland conversion to farmland, or partial transformations, such as forest-type changes [11].

Human activities have extensively utilized land for various purposes. The need for food, housing, and energy driven by population growth has led to the expansion of land use in the arid and semiarid regions of developing countries [12,13]. Over the years, many countries have been concerned about LULC changes due to population growth, migration, and urbanization [14,15]. Advances in remote sensing (RS) data collection and classification methods have accelerated research in this field. Specialists are increasingly using advanced RS and geographic information system (GIS) for spatiotemporal analyses that require machine learning (ML) for Earth observations and RS communities [16].

Numerous studies have explored image classification and LULC change detection, offering insights into many of Earth's surface issues that concern social, economic, and environmental aspects. Examples include the growth of developed areas and shifts in vegetation over time. Typical uses of the usual approaches to nonparametric supervised ML classifiers include support vector machines (SVM), artificial neural networks (ANN), decision trees, K-Nearest Neighbor (KNN), and random forests (RF) [17–24]. In addition, extreme gradient boosting (XGBoost) is a relatively new technique used in LULC classification studies. It is a decision tree-based ensemble ML developed using a ground-boosting machine (GBM) algorithm [25]. The results of several studies indicate that these algorithms generally provide a higher accuracy than conventional parametric classifiers.

Few studies have been conducted to assess the performance of ML algorithms (MLAs) in LULC classification and change detection. This study is groundbreaking in the Kurdistan region, as it is the first to employ both traditional and innovative MLAs over an extended timeframe. This reveals notable shifts in LULC, particularly post-1991, which has been driven by political upheaval and popular resistance against the former government. These changes have led to significant population migration, with people returning to their villages to engage in agricultural and rebuilding efforts. Additionally, the geopolitical nature of the study area located between Iran in the east and Turkey in the north, makes the region economically important.

In a local context, the selected study area (northeast Erbil Province) has experienced significant transformations over the past 30 years, including population growth and economic progress, leading to the conversion of rangelands into developed and agricultural spaces. These changes occurred because of successive conflicts in the region, resulting in the relocation of people and the creation of new settlements in urban areas. This has resulted in demographic changes and improper use of rangelands, forests, and agriculture in

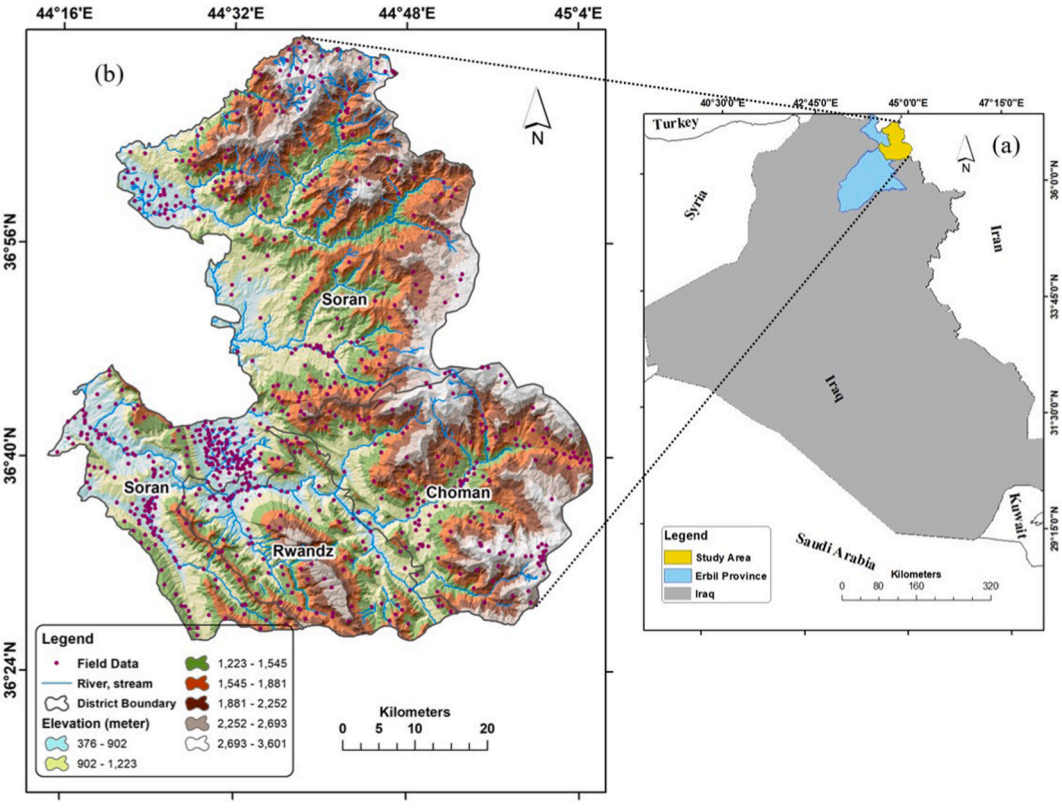

Fig. 1. Geographical location of the study area: (a) Iraq map, (b) Study area showing elevation, and field data.

both urban and rural areas [26]. Therefore, five MLAs were chosen for LULC classification mapping in this study for the aforementioned reasons. Some studies have already employed RS data classification methods to estimate the different types of LULC and the changes that have occurred in each type in the local districts of Erbil Province as a whole or in a particular study area.

Al-Hameedawi and Buchroithner [27] worked on object-oriented classification using Synthetic Aperture Radar and optical data from Erbil City. Hamad et al. [28] compared the maximum likelihood classification, RF, and two LULC classification methods on Landsat images of Halgurd Sakran National Park in 1998 and 2015. The high accuracy assessment values demonstrated the efficacy of RF classification in their research area. Mohammad et al. [29] studied urban changes in Erbil City using Landsat and Sentinel-2 images over three years (2000, 2010, and 2018). They applied a maximum likelihood classifier to generate LULC maps and determined the specific changes that occurred. Khwarahm et al. [30] investigated past, current, and future LULC change detection over three years (1988, 2002, and 2017). In addition, a maximum likelihood classifier was used to reveal the Landsat imagery LULC class categories in Erbil Governorate.

The primary objectives of this study were twofold. First, it aims to utilize and implement advanced MLAs to generate an LULC map, and subsequently determine the most effective algorithm for this task. Second, it intends to assess and quantify the spatial changes in LULC within a specific region over the past 30 years (1991–2021). The outcomes of this research will provide valuable insights to decision-makers, enabling them to comprehend the extent of changes in the study area and make informed decisions based on these findings.

2. Study area and datasets

2.1. Study area

The designated study area encompasses a total land area of 3547.5 km^2 and, comprises three districts: Soran, Choman, and Rwandz. Geographically, it is situated in the northeastern region of Erbil Province in the Kurdistan Region of Iraq, spanning 44° 14′ 44″–45° 05′ 25″ E and 37° 11′ 37″–36° 26′ 7.8″ N. The study area features mountainous terrain with diverse topographical attributes, including valleys, plains, hills, and high mountains, with elevations ranging from 378 to 3601 m (Fig. 1). This area has a diverse vegetation cover, including rangelands, forests, and riparian zones. Rangelands consist of grasslands and bushes, whereas mountain forests primarily contain oak trees. Riparian zones, along with river and stream banks, mainly include willows, maples, walnuts, and poplar trees [31].

The selected region exhibits a semi-arid climate characterized by scorching and arid summers alongside cold and rainy winters. However, mountainous regions with higher elevations display Mediterranean climate patterns as determined by the Köppen climate classification [32]. The recorded average annual temperature ranges from −6 °C to 46 °C, while the mean annual precipitation is approximately 700 mm.

In 1991, data on the distributions of rural and urban populations were limited. Interviews with elderly individuals and local authorities revealed that many villages have been destroyed, leading to forced migration and resettlement. The Fall of Baghdad in 2003 triggered a reversal of migration patterns, with people returning to their villages and resuming reconstruction efforts [33]. In 2020, the population of the study area was 267788, with 65 % living in urban areas and 35 % living in rural areas [34]. Changes in land cover and population distribution have led to the selection of this region, making it challenging to classify land types because of urban expansion and vegetation cover.

2.2. Datasets

This study used satellite imagery with a spatial resolution of 30 m from Landsat 5 (TM) and Landsat 8 (OLI) over three decades (1991–2021). Landsat 5 images were selected for 1991, 2001, and 2010, and Landsat 8 images were obtained for 2021. These images were used to generate LULC maps of the study area. During the study period, eight cloud-free Landsat satellite images, specifically from path/raw 169/34 and 169/35, were downloaded from the United States Geological Survey (USGS) (http://earthexplorer.usgs.gov/). A digital elevation model (DEM) with a resolution of 30 m was acquired from the Shuttle Radar Topography Mission (SRTM). Table 1 depicts the satellite images used in this study, which were acquired during the summer (July).

The supplementary data sources utilized in this study included archived high-resolution Google Earth images, ESRI ArcMap base maps, and the expertise of local individuals. These resources were employed to generate the training and validation data. In addition, a field survey was conducted in 2021 for on-site data collection. A handheld GPS device (GARMIN Montana 680) was employed to record the 810 sample points utilized in the subsequent training and validation processes. Because incorporating additional variables into

Table 1
Satellite images used in this study.

Satellite Sensor	No. of Images (Scenes)	Date of Acquisition	Bands	Path/Rows
Landsat 5 TM	2	July 21, 1991	1,2,3,4,5,7	169/34,35
Landsat 5 TM	2	July 16, 2001	1,2,3,4,5,7	169/34,35
Landsat 5 TM	2	July 09, 2010	1,2,3,4,5,7	169/34,35
Landsat 8 OLI	2	July 23, 2021	1,2,3,4,5,6,7	169/34,35
NASA SRTM DEM	4	Sept, 2014	Single band	N36E044,045 N37E044,045

digital image classification improves LULC classification [35], this study incorporated the DEM and normalized difference vegetation index (NDVI) obtained from the near-infrared (NIR) and red (R) bands of Landsat to enhance the accuracy of the results.

3. Methodology

In this study, GIS- and RS-based techniques were applied to classify and analyze the LULC dynamics. This study involves image preprocessing, supervised classification, and change detection. An accurate statistical analysis of the LULC changes in the study area

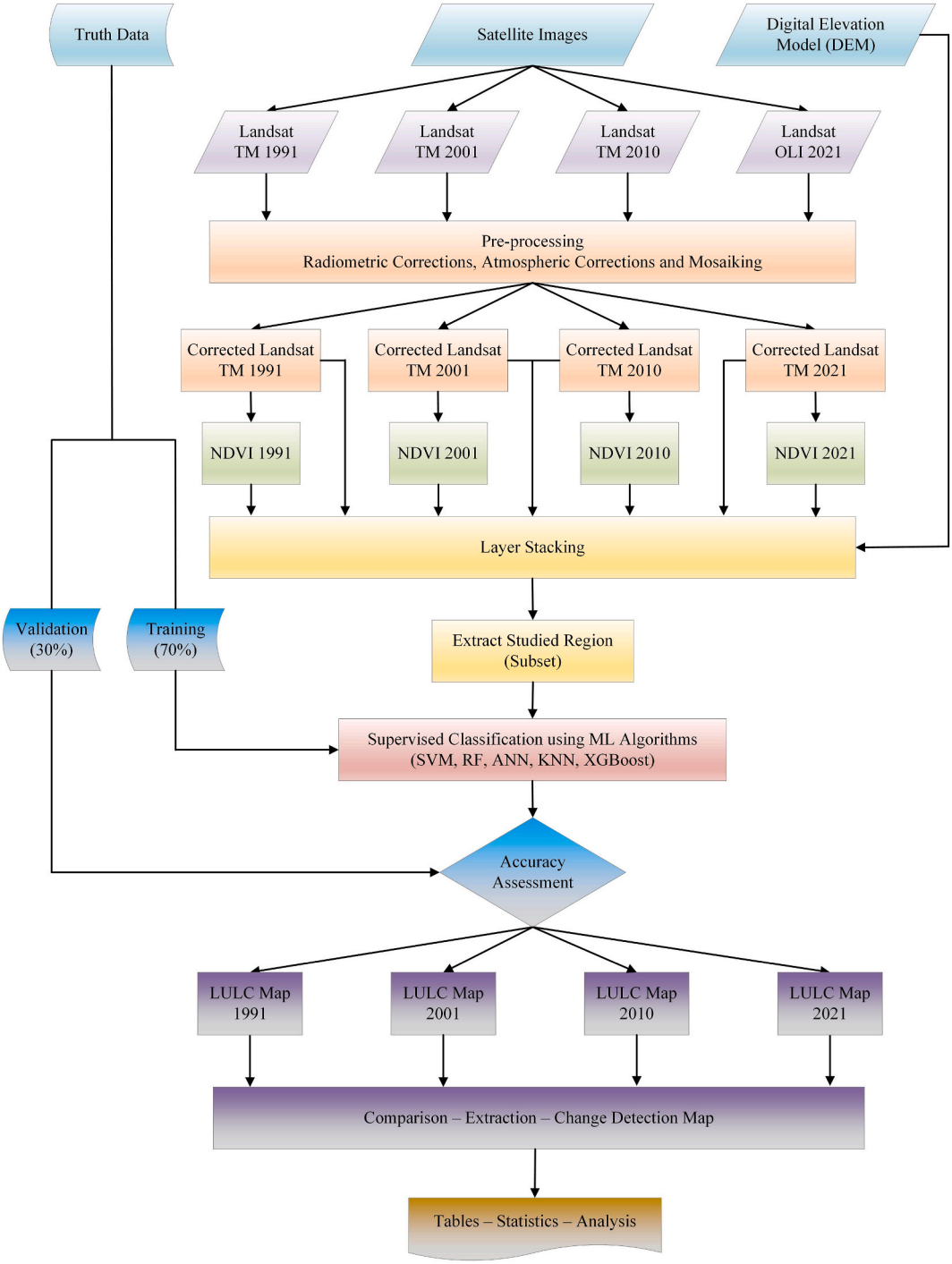

Fig. 2. Flowchart of the data processing.

was conducted. The methodology adopted in this study is summarized in Fig. 2.

3.1. Image preprocessing

Preprocessing the satellite images is an essential step prior to image classification and change detection because it mitigates the influence of the sensor, atmospheric, and topographic factors [36]. Within the scope of this study, several image preprocessing procedures were employed, including radiometric corrections, atmospheric corrections, and mosaicking using ENVI v5.3 software. A radiometric correction tool was used to address radiometric errors. Subsequently, atmospherically corrected and calibrated radiance values were obtained using the fast line-of-sight atmospheric analysis of spectral hypercubes atmospheric correction algorithm [37]. The process of mosaicking and image subsets was then implemented, and the spectral NDVI for all images was applied. All data were subsets within the study area shapefile and geometrically unified to the projection of the UTM 38 N and WGS-84 coordinate systems. DEM extraction for the study area was performed using ArcMap v10.8.2.

3.2. LULC classification method

The classification of the LULC categories in this study followed the widely recognized classification system introduced by Anderson [38]. This classification system was particularly suitable for this study because of its extensive geographical scope and spatial resolution of 30 m. The LULC type was selected on the basis of the specific physical characteristics of the study area. The eight classes encompassed in the classification were as follows: (1) agricultural land, (2) barren land, (3) built-up areas, (4) forests, (5) rangelands, (6) riparian forests, (7) snow-covered areas, and (8) water bodies. A detailed explanation of each class is provided in Table 2.

High-level techniques are recommended for constructing classification procedures to make high-level decisions when interpreting remotely sensed data [39]. ML can significantly improve the efficiency and time-saving classification of remotely sensed images [19]. Consequently, five pixel-based nonparametric MLAs were developed and evaluated in terms of the accuracy with which they solved the identified issues. Classification layers were created using a supervised classification method with MLAs. After using the algorithms to classify the study area, the best algorithm was selected for change detection analysis based on its accuracy and acceptable kappa. The classification process and assessment of MLAs were implemented using the R programming package [40].

3.3. MLAs

Modern technologies, such as ML approaches, which are a branch of artificial intelligence, are applied to the interpretation of RS data and earth observation studies and are relied upon by data scientists and decision-makers. This is because these techniques have already been proven effective in resolving problems and reducing timeframes [41]. For LULC classification and change detection, freely available satellite images and enhanced algorithms yield reliable results [42,43]. The following supervised MLAs were selected for the classification system and assessments and applied to the area of interest.

3.3.1. SVM

SVMs are nonparametric supervised statistical learning methods that do not assume the underlying distribution of a training dataset. They have been widely adopted owing to their attractive characteristics and strong empirical performance [44]. SVMs use a nonparametric technique with kernel functions to regulate a hyperplane that separates a dataset into predefined classes consistent with the training data. This approach is powerful for solving classification problems in MLAs and was introduced by Vapnik [45]. SVMs are popular in RS because they often outperform conventional methods in terms of classification accuracy, even with smaller training datasets [46]. However, the performance of SVMs can vary depending on the kernel type used [47].

3.3.2. KNN

The KNN algorithm is a valuable nonparametric approach that is widely used for the classification of various datasets [48]. An appropriate K value is determined by the employed metrics and varies when switching between datasets. Its advantages, such as the quick inclusion of data from beyond the study region, make it popular for classifying large-area RS data [49,50]. This method assigns a training sample to a predefined class label. Moreover, the KNN method, which uses georeferenced and remotely sensed field data, enables spatially continuous predictions [51].

Table 2
Description of LULC classes.

Class Type	Description
Agricultural Land	Agricultural croplands, cultivated lands, and agricultural fallow lands
Barren Land	Bare exposed rock and soil, un-vegetal land, degraded lands, and mixed barren land
Built-up	Areas selected as residential, commercial, industrial, and transportation facilities
Forest	Deciduous natural forest land, evergreen trees, mixed forest land
Rangeland	Herbaceous rangeland, shrubs, grassland, mixed rangeland
Riparian Zone	Riparian vegetation and riparian forestry
Snow	Perennial snow areas
Water	Rivers, streams, and ponds

3.3.3. ANN

ANNs, also known as neural networks, have been successfully applied to the study of RS images since the 1990s [52,53]. These nature-inspired algorithms represent complex data and are widely used in artificial intelligence for tasks ranging from regression to classification. ANNs consist of interconnected nodes, each with input and output connections and carry weighted information [54,55]. Their superiority over traditional methods has led to their rapid adoption in RS [56,57].

3.3.4. RF

Currently, some of the most widely used MLAs are RFs. The adaptability of this algorithm as a classification and regression tool for categorical and continuous data is a major factor in its success [58]. In addition, the RF algorithm is an integrative classifier, which is a reasonable option for LULC classification systems in RS [59]. This algorithm originally explains a set of predictors for a forest, in which each tree is predicted based on the values of a random vector drawn from the same distribution [60]. The RF classifier ensemble has the potential to increase RS image classification consistency and accuracy [61]. To accurately map various types of LULC, RS-based land cover monitoring requires reliable classification algorithms. The ability to assess the importance of variables and their nonparametric nature is the main advantage of RF [62].

3.3.5. XGBoost

In recent years, the XGBoost algorithm has emerged as a dominant force in applied ML, significantly affecting field GBMs owing to the rapid speed of its model execution and overall performance [63]. Its popularity stems from its superior performance compared with other GBMs. XGBoost is a subtype of gradient boosting that addresses regression and classification tasks using an ensemble of weak prediction models. Each model aims to rectify the weaknesses of its predecessors. Notably, XGBoost employs a pre-sorted technique to estimate the optimal splits in a dataset, ensuring the efficient handling of missing values and reducing overfitting. The integration of the gradient descent technique and leaf-wise pruning strategy contributes to minimizing errors and achieving optimal results [64].

3.4. Accuracy assessment

The most important step in image classification is accuracy assessment, which compares classification with reference field data to assess how well the classification represents the actual world [65,66]. The performance of a test sample is typically the focus of accuracy assessment using an error matrix. The resulting matrix allows us to compute the most popular measures of accuracy, including the overall accuracy (OA) and kappa coefficient (Kc) equations (3) and (4) [67].

Other measures of accuracy can be calculated, such as user accuracy (UA) equation (1), which indicates the proportion of pixels that are correctly classified within the image and represents the mutual error of commission. The producer accuracy (PA) equation (2), which is the probability that a pixel is correctly classified as a LULC type, is the mutual error of omission. The OA was calculated as the number of correctly categorized pixels divided by the total number of pixels used for evaluation [65]. More specifically, Kc is a standard statistical indicator used to measure classification precision. The Kc measures the classification accuracy of a randomly selected value [68]. Accuracy measurements were computed using the following equations:

$$UA = x_{ii}/x_{i+} \tag{1}$$

$$PA = x_{ii}/x_{+i} \tag{2}$$

$$OA = \sum_{i=1}^{r} x_{ii} \Big/ N \tag{3}$$

$$Kc = \left(N \sum_{i=1}^{r} x_{ii} - \sum_{i=1}^{r} (x_{i+} \times x_{+i}) \right) \Big/ \left(N^2 - \sum_{i=1}^{r} (x_{i+} \times x_{+i}) \right) \tag{4}$$

where N is the total number of samples, r is the number of LULC classes, xii is the number of observations, and xi+ and x + i are the marginal totals for row 'i' and column 'i' respectively. Kc values > 0.80 reveal a high degree of agreement between the ground reference data and classification map information, 0.40–0.80 imply reasonable agreement, and <0.40 indicates low agreement [69]. In this study, an accuracy assessment of the generated classified images was performed to examine the quality of information produced from the data using reference samples. Seventy percent of the samples were chosen for training and 30 % were chosen for testing by random sampling. This evaluation was performed using the R programming language package.

3.5. Change detection method

Change detection is a valuable technique for quantifying temporal changes in multi-temporal images or any given area over time [70,71]. The application of change detection has proven beneficial in monitoring environmental conditions and aiding in the identification of potential problems, which in turn can inform effective development strategies concerning LULC changes [72]. The accuracy of LULC change detection relies on precise classification mapping [73,74], enabling the tracking and quantification of such changes. RS data serve as a valuable resource for determining the magnitude of change, as is evident from the discernible differences between two images captured at distinct points in time [75].

In this study, the finest ML classifiers were employed to classify Landsat images and generate LULC maps. The resulting maps facilitated the quantification of changes (km [2]) for each LULC class during the periods 1991–2001, 2001–2010, and 2010–2021. This was applied to the RS and GIS software, Quantum GIS (QGIS v3.28). Within QGIS, change detection maps and statistics were produced using the semi-automatic classification plugin.

4. Results and analysis

4.1. LULC classification maps and accuracy evaluation

In this study, we applied and evaluated five supervised MLAs to datasets from 1991, 2001, 2010, and 2021. The study area was categorized into eight classes: agricultural land, barren land, built-up area, forest, rangeland, riparian forest, snow, and water. Fig. 3 illustrates the classified maps generated by the five MLAs for the aforementioned years. Notably the most prevalent class in the study area was rangeland. This is primarily because of the mountainous terrain of the region, which has been inaccessible to the public since the previous regime. Consequently, the majority of the rural population has migrated to urban areas, resulting in rangeland dominance.

To assess the accuracy of the classified LULC maps, an error matrix was calculated. The OA and Kc values were calculated for each LULC classification using all classifiers. Approximately 238 points were tested against 572 reference samples in 2021 obtained from field surveys, Google Earth, and interviews for each classified map. The allocation of points for assessing different land classes across all years is shown in Table 3. The error matrices of the ML classifiers are listed in Table 4. Furthermore, the evaluation identified correct and incorrect validation samples as well as determined the PA and UA.

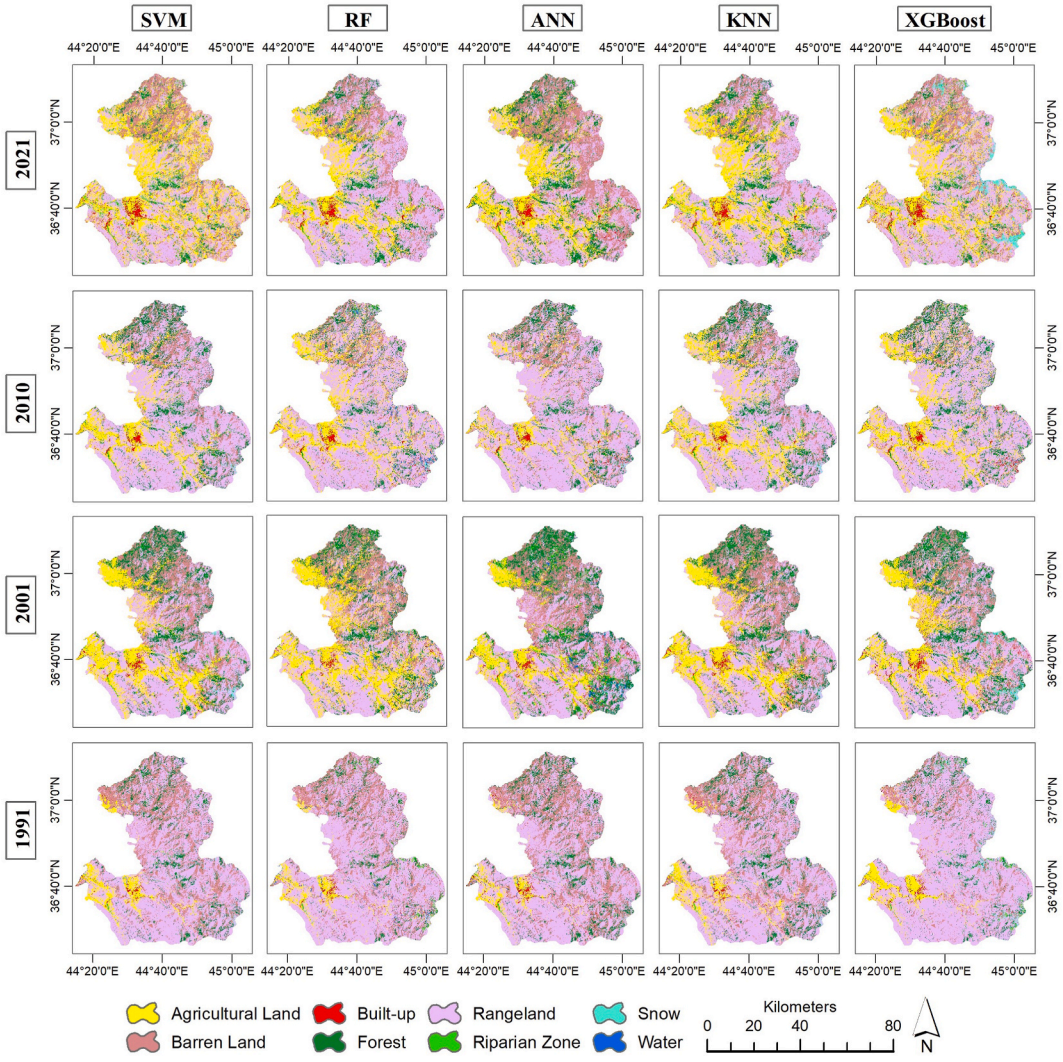

Fig. 3. LULC Classification maps using five MLAs (SVM, RF, ANN, KNN, and XGBoost) from 1991 to 2021.

Table 3
Total yearly allocated sample points divided into training and validation points.

Years	Sample Points	Training data 70 %	Validation data 30 %
1991	634	448	186
2001	671	473	198
2010	720	508	212
2021	810	572	238

Despite the complex nature of the study area, which was classified into eight distinct LULC categories, the LULC maps generated by the five MLAs demonstrated high-accuracy assessment results. The algorithms displayed noteworthy performances, with the RF classifier achieving the highest OA of 97.47 %, whereas the ANN classifier achieved the lowest OA of 92.47 %. Fig. 4 illustrates the highest and lowest OA achieved by all MLAs across all years.

Because of the LULC spectral characteristics and varied algorithm performance, a consistent pattern was identified in the accuracy of the mapping categories [76]. However, in 2010, higher accuracy was recorded by the ANN and SVM algorithms (Fig. 4); both classified most categories as more accurate, with higher PA, particularly in the agricultural land and rangeland classes. Additionally, the sample size and quality of the training data may significantly influence the classification [19].

Furthermore, compared with alternative algorithms, the RF algorithm demonstrated superior OA. It also exhibited better performance in terms of individual class accuracy, as evidenced by higher PAs and UAs across all LULC classes (Table 4). The resulting Kc values ranged from 0.91 to 0.97, indicating a high level of agreement with the reference LULC categories [69]. Based on these findings, the RF algorithm was selected as the optimal method for LULC classification in the study area (Fig. 5). Therefore, this algorithm was employed for the statistical analysis of LULC change detection over the study period.

4.2. The variable importance valuation

Assessing variable importance is crucial for datasets with high variables, and using only essential features can improve classification accuracy [19]. To classify LULC using MLAs, this study used spectral values from satellite imagery as input variables [77]. Additionally, the DEM was incorporated as an input variable in the classification process, primarily to reduce misclassification in shaded regions [39,78].

The accuracy of the overall classification was affected by the difficulty in identifying vegetation. To address this problem, a previous study reported consistency among several spectral indices [79]. Among these spectral indices, NDVI plays a vital role in classifying LULC categories associated with vegetation owing to its strong correlation with green vegetation.

Fig. 6 illustrates the importance of RF input variables for each LULC class in 2021. The features considered were the Landsat 8 OLI bands, NDVI, and DEM. B5 (NIR) and NDVI were identified as the most effective variables for vegetation cover, including riparian zone, forest, and agricultural land. This finding is consistent with the recognition of the usefulness of USGS Landsat bands (https://www.usgs.gov/faqs/what-are-best-landsat-spectral-bands-use-my-research/).

The identification and inclusion of the most significant features, which account for a substantial portion of the variance in the response variable, are crucial for the development of effective and high-performing models [80]. The study reveals that variable importance is the most significant factor in categorizing variables, with auxiliary variables like NDVI and DEM enhancing classification accuracy. Despite a constant distribution of LULC types and NDVI values, NDVI remains significant.

The analysis reveals that the original NIR band (B5) and NDVI significantly influence classification outcomes, possibly due to the unique values of land cover types in the study area. Furthermore, the examination of these characteristics aids in mitigating the inaccuracies associated with classifying diverse terrain surfaces [79]. The riparian zone has the lowest reflectance values among vegetation classes, except for bands 5 and NDVI. Blue bands, such as B2, differentiate between types. Blue light reflection is low in forested and riparian zones, but higher in snow-covered and built-up areas.

In general, the contributions of the remaining bands varied in importance ranking for specific LULC categories. For instance, the B6 (SWIR1) and elevation variables were recorded as relatively important in the rangeland class, which aligns with the findings of a previous study [20]. B1 and B2 (blue) contributed highly to the built-up area class, conferring to the study Yu et al. [81], bands B1 and B2 in Landsat 8 OLI had the strongest correlation compared with other pairs of bands. The variable importance results for 1991, 2001, and 2010 obtained using the RF algorithm are shown in Figs. S1–S3.

Even features that contribute less, such as B2, can be useful for determining the differences between classes. For instance, the reflectance of blue light is low in both vegetation and water but significantly higher in barren land and built-up areas [82]. Another significant factor is the sensitivity of the shortwave infrared to variations in the leaf moisture content and surface wetness [83]. This sensitivity enabled the classification of LULC categories, such as forests, rangelands, and open water, based on their distinct moisture profiles. For example, in NDVI, Bands 5 and 6 contributed significantly to the water spectral patterns. All variables contributed to the spectral reflectance of the snow cover, except for B5, which had a lower impact.

The importance of the features was calculated, revealing that bands 5 and 6 made the highest contributions, making them more effective for LULC classification in the study area. The relevance of the satellite images and other variables followed the descending order of B5 > NDVI > B6 > B2 > DEM in the RF algorithm. Overall, variables B5, B6, and NDVI were considered significant features, indicating their substantial influence on the classification outcomes. This can be attributed to dimensionality, which suggests that the number of predictors affects the accuracy of the LULC classification predictions.

Table 4
Accuracy assessment of LULC classes using MLAs from 1991 to 2021.

	MLAs	Accuracy	AL	BL	B	F	RL	RZ	S	W	OA	Kc
1991	**SVM**	**PA**	94.44	92.59	100	89.13	89.47	95.5	100	100	93.01	0.917
		UA	80.95	96.15	83.33	97.62	100	80.77	100	100		
	RF	**PA**	88.89	92.59	100	91.3	94.74	95.45	100	100	94.09	0.93
		UA	84.21	100	90.91	97.67	94.74	84	100	100		
	ANN	**PA**	83.33	88.89	90	93.48	92.11	95.45	100	100	92.47	0.91
		UA	78.95	100	75	97.73	92.11	87.5	100	100		
	KNN	**PA**	77.78	92.59	100	93.48	94.74	90.91	100	100	93.01	0.92
		UA	82.35	96.15	90.91	95.56	90	90.91	100	100		
	XGBoost	**PA**	83.33	92.59	100	91.3	94.74	90.91	100	100	93.01	0.92
		UA	88.24	96.15	100	95.45	92.31	80	100	100		
2001	**SVM**	**PA**	73.68	96.15	92.86	98.04	95.24	100	100	90	94.44	0.933
		UA	77.78	100	81.25	100	93.02	95.65	100	100		
	RF	**PA**	78.95	100	93.33	100	100	100	100	100	97.47	0.97
		UA	93.75	100	87.5	100	95.45	100	100	100		
	ANN	**PA**	80	100	81.25	100	95.24	95.65	100	100	94.95	0.94
		UA	88.89	92.31	86.67	100	93.02	95.65	100	100		
	KNN	**PA**	84.21	96.15	93.33	100	95.24	100	100	100	96.46	0.96
		UA	80	100	87.5	100	97.56	100	100	100		
	XGBoost	**PA**	73.68	96.15	93.33	100	97.62	100	100	100	95.96	0.95
		UA	93.33	100	82.35	100	91.11	100	100	100		
2010	**SVM**	**PA**	85.71	96.3	100	97.87	95.65	100	100	88.89	96.23	0.955
		UA	94.74	92.86	100	97.87	93.62	96.3	100	100		
	RF	**PA**	80	100	95.24	100	95.74	100	100	66.67	95.28	0.94
		UA	88.89	89.66	95.24	100	91.84	100	100	100		
	ANN	**PA**	90	92.31	100	97.92	97.87	100	100	88.89	96.7	0.96
		UA	90	100	95.45	100	93.88	96.3	100	100		
	KNN	**PA**	80	92.31	100	97.92	95.74	96.15	100	100	95.28	0.94
		UA	80	100	100	100	90	96	100	100		
	XGBoost	**PA**	85	92.31	90.48	100	95.74	96.15	86.67	66.67	92.92	0.92
		UA	73.91	88.89	95	97.96	93.75	100	100	85.71		
2021	**SVM**	**PA**	92.59	96.67	100	96.23	96.08	96.15	90	100	96.25	0.95
		UA	92.59	96.67	97.14	98.08	94.23	96.15	100	100		
	RF	**PA**	93.3	90	97.06	94.34	100	100	100	100	96.67	0.96
		UA	96.3	96.43	94.29	98.04	98.08	92.85	100	100		
	ANN	**PA**	96.3	86.67	97.06	98.11	94.12	100	100	100	95.83	0.95
		UA	86.67	96.3	94.29	100	97.96	96.3	100	90		
	KNN	**PA**	86.67	87.5	100	96	95.83	96.15	90.91	100	94.17	0.93
		UA	89.66	100	94.44	92.31	92	96.15	100	100		
	XGBoost	**PA**	85.71	100	94.44	96.08	100	96.15	90	100	95.83	0.95
		UA	100	96.77	100	96.08	94.34	92.59	100	100		

AL: Agricultural land, BL: Barren land, B: Built-up area, F: Forest, RL: Rangeland, RZ: Riparian zone, S: Snow, and W: Water.

4.3. LULC change detection analysis

Detecting changes across multi-temporal images over time requires a post-classification process that allows for pixel-based comparisons. Classified maps must be categorized appropriately [70,73].

Table 5 and Fig. 7 present the results obtained from the RF algorithm within the selected time frame from 1991 to 2021. The statistical analysis of LULC quantities revealed significant changes in the rangeland and agricultural land classes during this period. Notable changes were also observed in the barren land, forests, and built-up areas. However, relatively smooth changes were identified in the riparian zone, snow, and water classes.

Specifically, the area of the rangeland class decreased from 2370.02 km^2 in 1991 to 1435.68 km^2 in 2001, which can be attributed to the people returning to their lands and villages. Consequently, the agricultural land class expanded from 137.02 to 813.94 km^2, whereas built-up areas increased from 25.31 to 34.87 km^2 over the same period. In addition, the forest class experienced rejuvenation, growing from 167.73 to 447.99 km^2. Conversely, barren land remained relatively stable, with a slight decrease from 774.76 to 730.14 km^2. The riparian zone exhibited minimal changes, with its area fluctuating slightly from 45.86 to 45.89 km^2. The snow and water classes, however, demonstrated an increase due to favorable climate conditions during that time, expanding from 2.95 to 10.72 km^2 and 23.85–28.29 km^2, respectively.

Over the same time frame, agricultural land significantly decreased from 813.94 km^2 in 2001 to 531.56 km^2 in 2010, as farmers abandoned their land to pursue employment opportunities in the government and security sectors. The forest area also suffered a notable decline, plummeting from 447.99 to 243.28 km^2 due to deforestation driven by the demand for charcoal and firewood as alternative fuel sources. In contrast, built-up areas expanded from 34.87 to 42.94 km^2 due to population growth and urbanization. Moreover, the rangeland and barren land categories experienced an upward trend, growing from 1435.68 to 1806.72 km^2 and 730.14–839.69 km^2, respectively.

From 2010 to 2021, significant changes in vegetation cover were observed across various land categories. Agricultural land, forest,

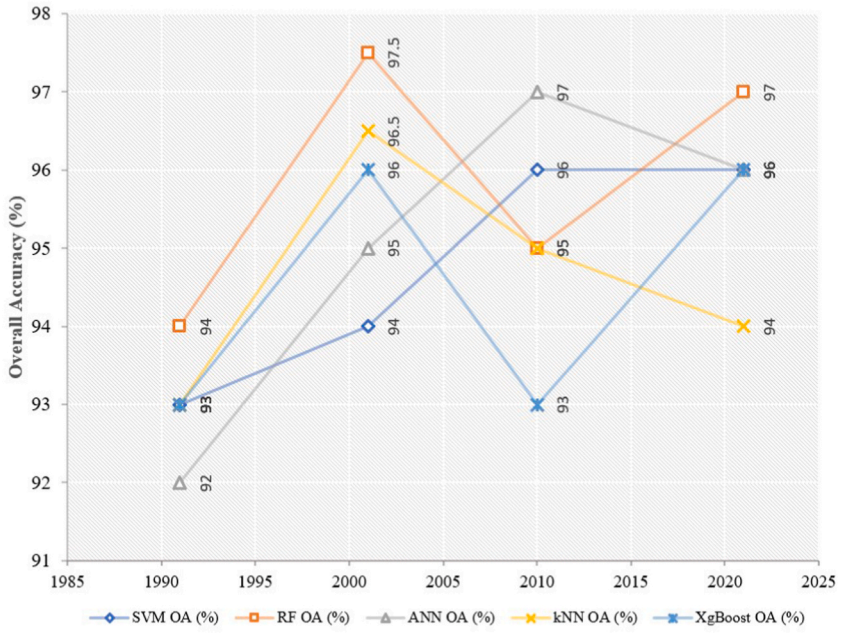

Fig. 4. The OA percentage values of MLAs from 1991 to 2021.

rangeland, and riparian zones all expanded, increasing from 531.56 to 617.2 km^2, 243.28–289.48 km^2, 1806.72–1967.99 km^2, and 42.54–57.38 km^2, respectively. Built-up land also increased from 41.94 to 50.52 km^2. Conversely, the barren land class decreased from 839.69 to 537.96 km^2.

By examining the LULC classification maps and associated attribute tables for 1991, 2001, 2010, and 2021, the shifts in each land category were identified and quantified. Table 6 presents the computed LULC changes for each class in each decade. The findings demonstrated that significant alterations occurred in the rangeland, barren land, agricultural land, and forest classes.

Agricultural land in the study area witnessed a gain of 19.08 % from 1991 to 2001 and 2.41 % from 2010 to 2021 but experienced a loss of 7.96 % from 2001 to 2010. Similarly, the forest class increased by 7.9 % from 1991 to 2001 and 1.3 % from 2010 to 2021, but decreased by 5.77 % from 2001 to 2010. Built-up land gained 0.27 % from 1991 to 2001, 0.2 % from 2001 to 2010, and 1.3 % from 2010 to 2021.

In contrast, rangelands experienced a substantial decline of 26.34 % from 1991 to 2001 but displayed a rapid increase of 10.46 % from 2001 to 2010, followed by a 4.55 % increase from 2010 to 2021. Fig. 8 further illustrates the analysis of net change detection, revealing a notable increase of 13.54 % in agricultural land and a positive change of 3.43 % in forest coverage over the three decades. Additionally, both built-up areas and riparian zones experienced gradual expansion, with increases of 0.71 % and 0.32 %, respectively.

However, the expansion of rangelands and barren lands occurred simultaneously with a decrease in their overall coverage. Rangelands experienced a loss of 11.33 %, while barren lands decreased by 6.68 %. Throughout the study period, the areas covered by snow or water bodies did not substantially change.

Table 7 presents the calculated net cross-transition changes among the different LULC classes, and Fig. 9 shows a chord diagram of these changes over the three decades. The change detection showed that within this period (1991–2021), 51.1 km^2 of the agricultural land remained unchanged, while 16.68 km^2 transformed into built-up areas, 12.39 km^2 turned into barren land, and 53.38 km^2 was converted into rangeland. Additionally, 0.39, 2.23, 0.66, and 0.18 km^2 transitioned to forests, riparian, snow, and water zones, respectively. This indicated a noticeable increase in agricultural land following the 30-year LULC transformation. In terms of built-up areas, 12.98 km^2 remained unaltered, while 7.78 km^2 became agricultural land. The built-up class exhibited minor changes in the other LULC categories. Concerning barren lands, 378.97 km^2 remained unchanged, while 148.26 km^2 was converted into agricultural land, 104.46 km^2 became forests, and 138.33 km^2 into rangeland. Additionally, small portions of 1.68 and 2.69 km^2 underwent changes in both built-up and riparian zone classes, respectively. Consequently, barren land decreased because of the other LULC types.

Analysis of the forest class revealed that during the study period, approximately 114.9 km^2 of forest land remained unaffected. However, 2.53 km^2 was converted to agricultural land, 17.35 km^2 was transformed into barren land, 28.02 km^2 became rangelands, and 4.78 km^2 was converted into riparian zones. Only 0.12 km^2 of forest land changed into built-up areas, while no significant changes were observed in snow cover and water bodies. Overall, these findings indicated an increase in forest land.

The rangeland category exhibited the most significant changes in terms of losses. Of the total rangeland area of 1722.26 km^2, the majority remained unchanged. However, 398.53 km^2 shifted to agricultural land, 18.5 km^2 transformed into built-up areas, 114.29 km^2 converted into barren lands, 75.63 km^2 changed to forest land, and 38.21 km^2 was transferred to the riparian zone. Additionally, 2.38 and 0.22 km^2 of rangeland changed into snow cover and water bodies. In the riparian zone, 9.1 km^2 remained unaffected. However, 1.45, 0.31, 0.79, 12.05, and 22.15 km^2 were converted to agricultural land, built-up areas, barren land, forest, and

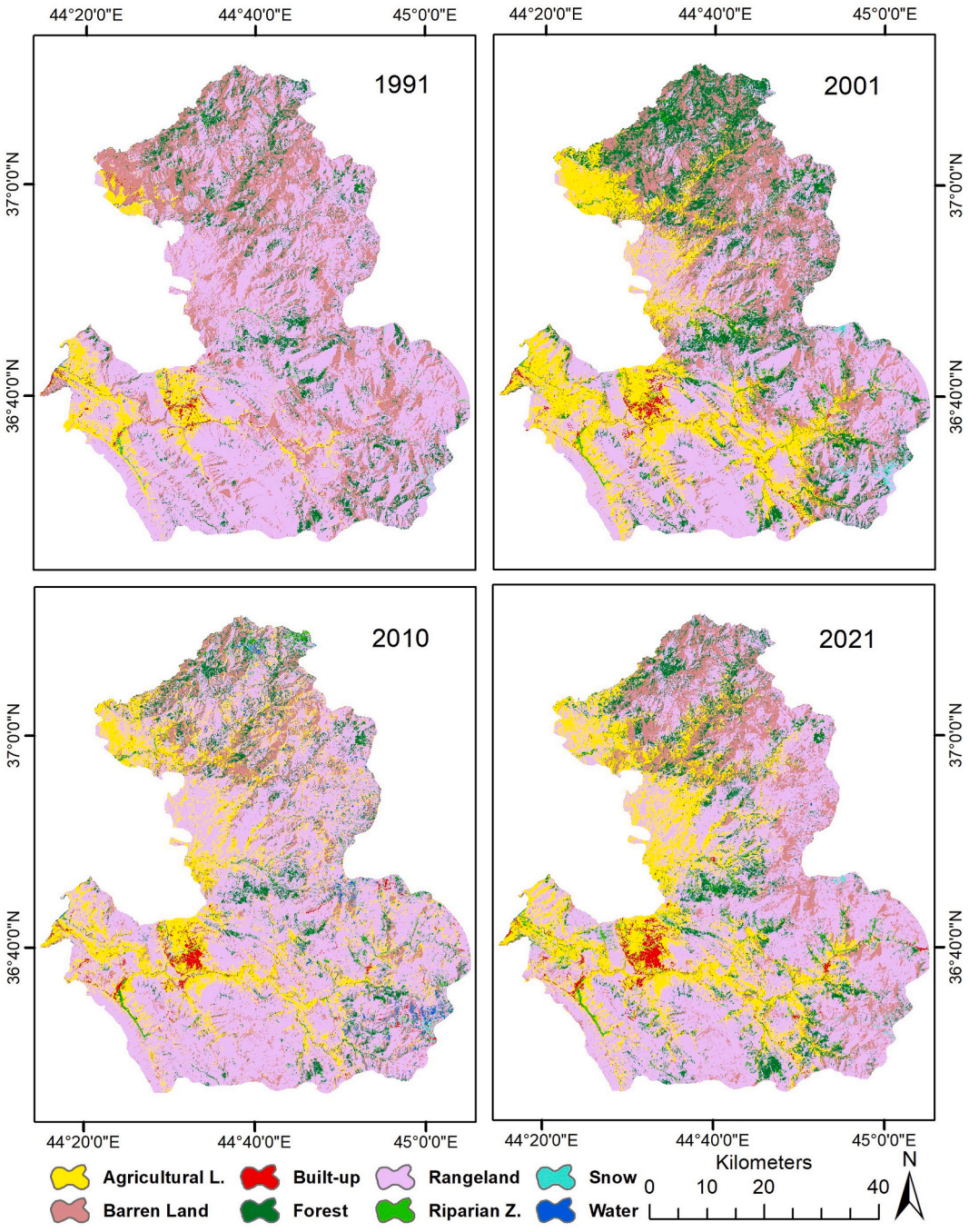

Fig. 5. LULC classification maps using the RF algorithm for different years (1991, 2001, 2010, and 2021).

rangeland, respectively. Minimal changes were observed in the snow cover and water bodies within this category.

Additionally, when examining the last two LULC categories, snow cover and water bodies remained stable at 1.16 and 1.96 km^2, respectively. However, there were alterations within the water class, with 7.55 km^2 transforming into agricultural land, 0.23 km^2 turning into built-up areas, and 12.03 km^2 converting into barren land. The ratios of 0.71, 0.98, 0.2, and 0.19 km^2 experienced shifts towards individual classes such as forest, rangeland, riparian zone, and snow cover. These changes indicated a decline in the water class within the study area by 2021.

Furthermore, considering the total transition within the entire study area, Table 7 shows that approximately 65 % or 2292.3 km^2 remained unchanged in terms of LULC in the selected study area over the three decades. However, these transitions can be visualized as a chord diagram. The chord diagram, a graphical method was utilized to statistically portray the flux transformation relationship

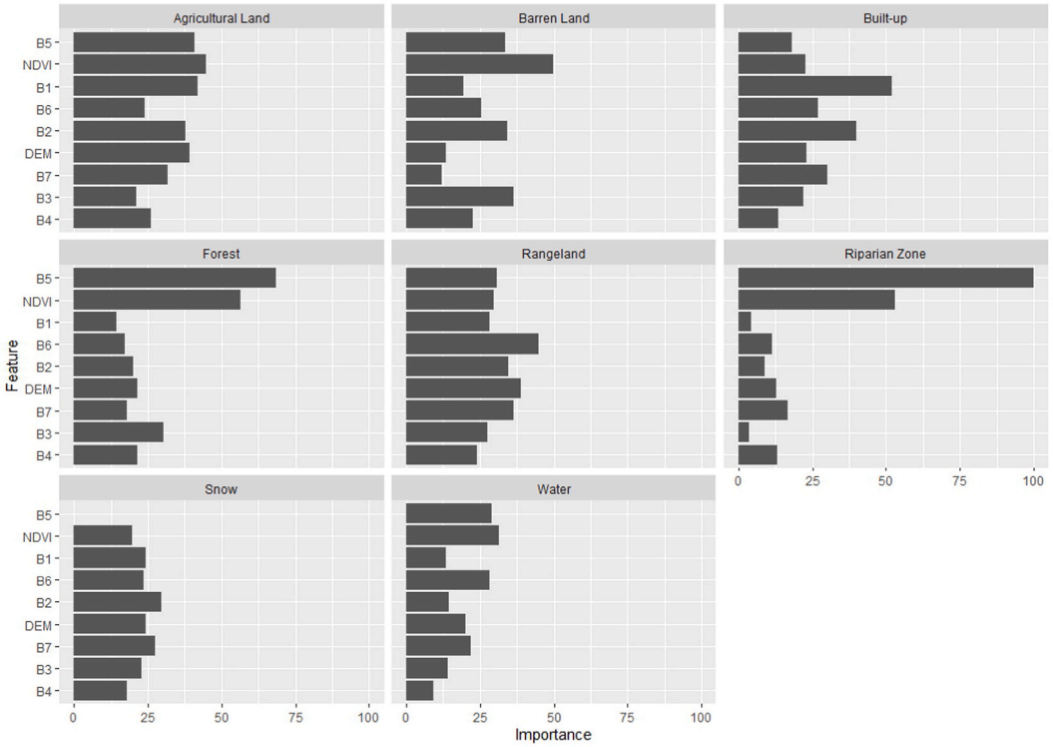

Fig. 6. Variable importance for each LULC category in 2021 using the RF algorithm.

Table 5
Land area class distribution (km [2]) and percentage (%) in the study area for the years 1991, 2001, 2010, and 2021.

Class type	1991		2001		2010		2021	
	Area km [2]	Area%	Area km [2]	Area%	Area km [2]	Area%	Area km [2]	Area%
Agricultural Land	137.02	3.86	813.94	22.94	531.56	14.98	617.20	17.40
Barren Land	774.76	21.84	730.14	20.58	839.69	23.67	537.96	15.16
Built-up	25.31	0.71	34.87	0.98	41.94	1.18	50.52	1.42
Forest	167.73	4.73	447.99	12.63	243.28	6.86	289.48	8.16
Rangeland	2370.02	66.81	1435.68	40.47	1806.72	50.93	1967.99	55.48
Riparian Zone	45.86	1.29	45.89	1.29	42.54	1.20	57.38	1.62
Snow	2.95	0.08	10.72	0.30	6.41	0.18	5.18	0.15
Water	23.85	0.67	28.29	0.80	35.37	1.00	21.80	0.61
Total	**3547.5**	**100**	**3547.5**	**100**	**3547.5**	**100**	**3547.5**	**100**

between LULC types over specified time periods, allowing for a clear description of the flow direction and diversity of LULC change. This diagram has been used by a variety of academics to construct transition matrices [84–86].

Fig. 9 represents the process of LULC transition in the study area from 1991 to 2021. The findings indicated that the observed increase in agricultural land (represented by the color yellow) was mostly due to the transformation of rangeland and barren land. The total area converted for this purpose amounted to 480.18 km2, which accounted for 13.54 % of the total area (see Fig. 8). The percentage of barren land (shown in brown) that was transformed into rangeland, forests, and agricultural lands is 6.68 %. The built-up area (shown in red) grew by 0.71 % due to the alteration in rangeland and agricultural lands.

The observed expansion of forested areas (shown in dark green) primarily results from the conversion of rangeland, barren land, and riparian zones, accounting for a 3.43 % increase. In contrast, an area of 402.03 km2 of rangeland (purple) underwent conversion into agricultural land, forest, and built-up areas. In addition, there was a marginal increase of 0.32 % in the riparian zone (shown in light green) as a result of the rangeland loss.

Overall, according to the LULC transfer trend analysis depicted in Fig. 9, it can be seen that rangelands exhibited the most significant alterations among all LULC categories. Rangeland undergoes primarily four forms of land transformation, namely conversion into agricultural land, forested areas, riparian zones, and built-up areas. Tables S1–S3 and Figs. S4–S6 separately provide the cross-transition tables and chord diagrams of each decade.

After post-processing in QGIS using the land cover change plugin, the two layers of the LULC maps were used to generate a

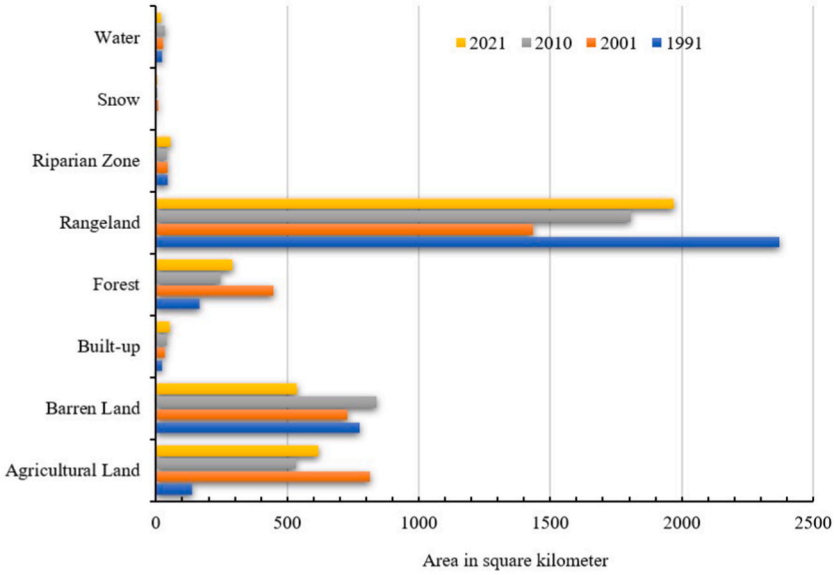

Fig. 7. LULC area classes for the years 1991, 2001, 2010, and 2021.

Table 6
Land change class distribution (km [2]) and percentage (%) in the study area for the decades 1991–2001, 2001–2010, and 2010–2021.

Class	1991–2001		2001–2010		2010–2021	
	Change area km [2]	Change%	Change area km [2]	Change%	Change area km [2]	Change%
Agricultural Land	676.92	19.08	−282.38	−7.96	85.64	2.41
Barren Land	−44.62	−1.26	109.55	3.09	−301.73	−8.51
Built-up	9.57	0.27	7.06	0.20	8.59	0.24
Forest	280.26	7.90	−204.72	−5.77	46.20	1.30
Rangeland	−934.34	−26.34	371.05	10.46	161.27	4.55
Riparian Zone	0.02	0.00	−3.34	−0.09	14.84	0.42
Snow	7.77	0.22	−4.31	−0.12	−1.24	−0.03
Water	4.44	0.13	7.08	0.20	−13.57	−0.38

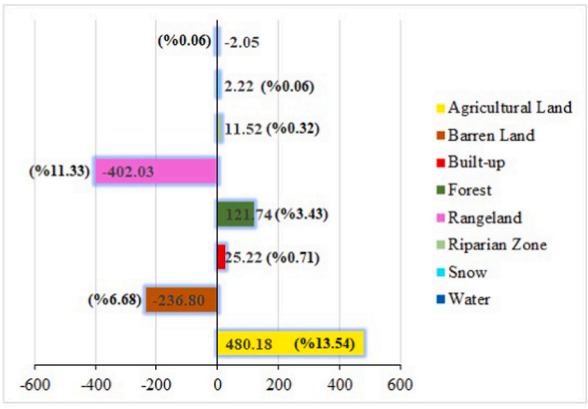

Fig. 8. LULC change detection (km [2]) from 1991 to 2021.

comprehensive representation of the spatial changes that occurred between 1991 and 2021. Fig. 10 shows the LULC classes that remained unchanged. All other converted classes are listed in Table 7, which illustrates the spatial mapping of the cross-transitions. The formation of these transitions corresponded to anthropogenic gathering and relocation along the main roads for easy transportation and commercial benefits. The Haj-Omran crossing border and trading gate are located between Iraq and Iran, specifically in the Choman District, southeast of the study area (Fig. 10).

Table 7
Cross-transition matrix of LULC changes (km [2]) in 1991–2021.

	LULC 2021										
LULC 1991	Class	AL	B	BL	F	RL	RZ	S	W	Total	No Change
	AL	*51.1*	*16.68*	*12.39*	*0.39*	*53.38*	*2.23*	*0.66*	*0.18*	*137.02*	*51.1*
	B	*7.78*	*12.98*	*1.3*	*0.03*	*1.97*	*0.17*	*0.74*	*0.34*	*25.31*	*12.98*
	BL	*148.26*	*1.68*	*378.97*	*104.46*	*138.33*	*2.69*	*0.04*	*0.31*	*774.75*	*378.97*
	F	*2.53*	*0.12*	*17.35*	*114.9*	*28.02*	*4.78*	*0*	*0.05*	*167.73*	*114.9*
	RL	*398.53*	*18.5*	*114.29*	*75.63*	*1722.3*	*38.21*	*2.38*	*0.22*	*2370*	*1722.26*
	RZ	*1.45*	*0.31*	*0.79*	*12.05*	*22.15*	*9.1*	*0*	*0.01*	*45.86*	*9.1*
	S	*0*	*0.02*	*0.83*	*0.03*	*0.9*	*0*	*1.16*	*0*	*2.95*	*1.16*
	W	*7.55*	*0.23*	*12.03*	*0.71*	*0.98*	*0.2*	*0.19*	*1.96*	*23.85*	*1.96*
	Total	*617.2*	*50.52*	*537.96*	*308.19*	*1968*	*57.38*	*5.18*	*3.08*	*3547.5*	*2292.43*

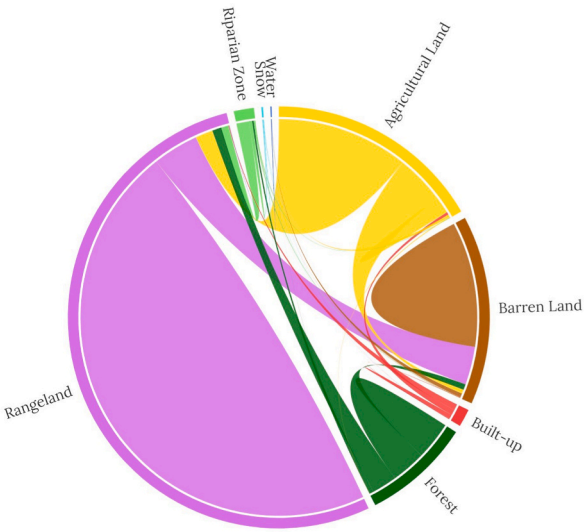

Fig. 9. Proportional LULC changes illustrated by chord diagram, 1991–2021.

Due to the necessity of human life, parts of the rangelands have been altered into agricultural and built-up areas, along with the reclamation of riparian zones. In addition, the expansion of agricultural land occurred in the Soran District, as indicated by the southwest, northwest, and city centers. The Rwandz district faced minor alterations in LULC because it is located on no main roads and is not under major human relocation compared with the other two districts.

5. Discussion

Assessing and tracking changes in LULC across large regions is essential in various fields, including climate change studies and natural resource management [87]. The accurate estimation of LULC maps generated from RS data is in high demand, particularly in areas with limited or no available LULC prevalence data [30]. The use of the five MLAs in this study uniquely enhanced the reliability and precision of the LULC classification and land change detection over a 30-year period from 1991 to 2021. This approach is especially noteworthy when compared with previous studies. For example, Ge et al. [20] applied four MLAs to extract LULC information in September 2017 in the Dengkou Oasis dryland regions in China. Abdi [42] examined four nonparametric algorithms for one year in each season in a complex mixed-use landscape in Sweden. Loukika et al. [87] used three different MLAs for 2016, 2018, and 2020 in the Munneru River Basin, India. Tariq et al. [23] implemented three ML techniques from 1990 to 2017 in Khyber Pakhtun Khwa, Pakistan. Atef et al. [88] applied three algorithms to investigate spatiotemporal land use changes in El-Fayoum Governorate, Egypt.

The effectiveness of MLAs varies depending on the specific application and characteristics of the training data [19]. We observed that the accuracies of most algorithms were similar. This is because properly fine-tuning algorithmic parameters can potentially lead to classification accuracies exceeding 90 % [18,20]. In this study, optimal parameter tuning was examined to attain higher performance: for instance, 'mtry' and 'ntree' parameters in the RF algorithm and 'K values' the number of neighbors in the KNN algorithm. XGBoost, an ensemble learning technique rooted in gradient boosting [25], particularly excels when dealing with high-resolution RS data and scales well with more training data [25]. This study showed that XGBoost achieved impressive accuracy levels between 93 % and 96 % when applied to medium-resolution RS images. However, the RF algorithm generally performed even better in the context of medium-resolution images.

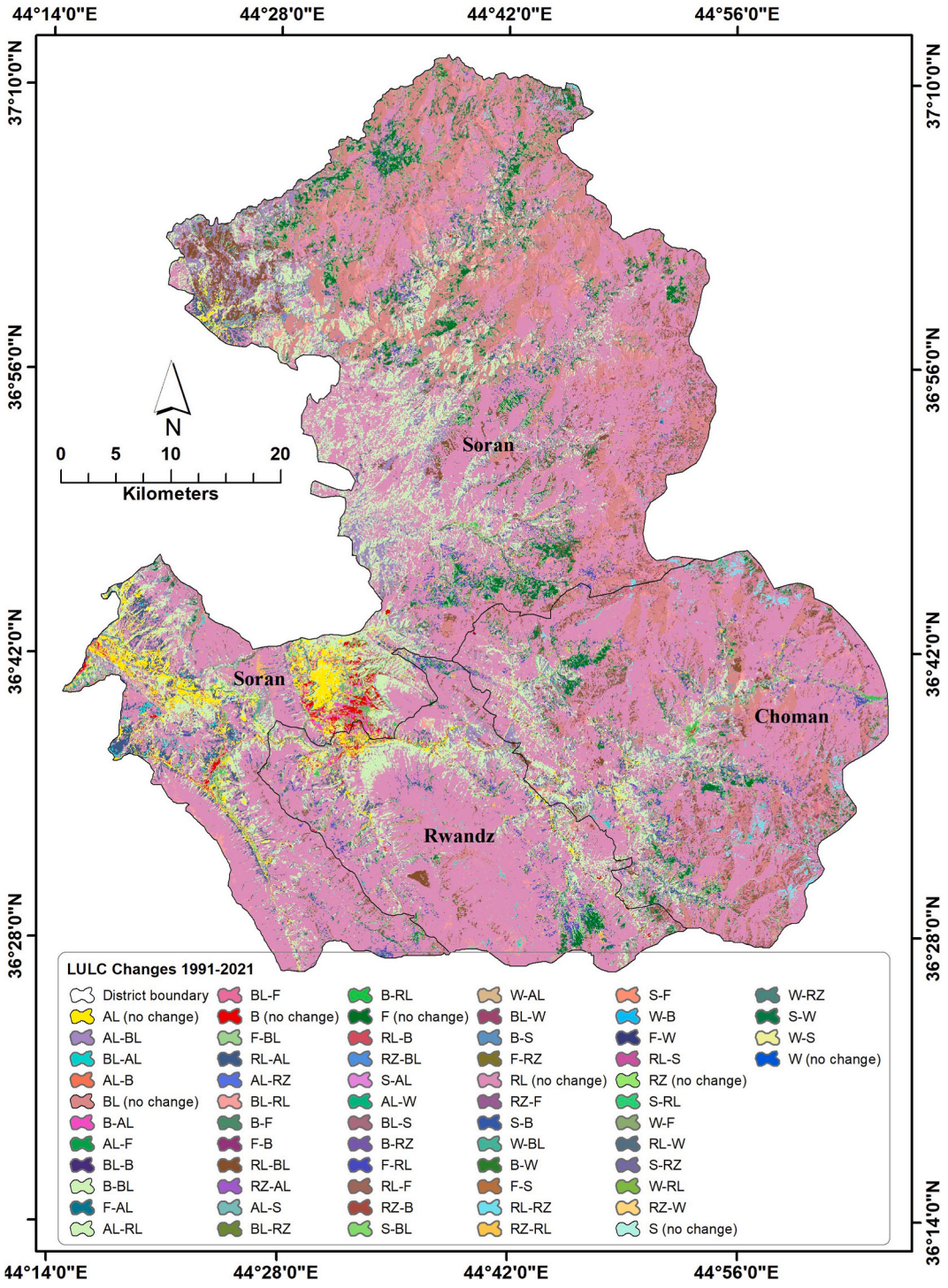

Fig. 10. LULC change map from 1991 to 2021 depicting alterations in AL (Agricultural land), BL (Barren land), B (Built-up areas), F (Forests), RL (Rangelands), RZ (Riparian zones), S (Snow), and W (Water).

In the realm of RS applications, algorithms invariably have inherent strengths and shortcomings. RF shows commendable robustness and is not significantly influenced by parameter changes, whereas SVM can be sensitive to hyperparameter adjustments. An ideal classification strategy, as suggested in the previous literature, must have low susceptibility, high comprehensiveness, and is fast [65]. RF has emerged as a reliable method for gauging the relevance of variables and classifying LULC types. Notably, bagging and random subspace selection are two instrumental techniques in the field of RF algorithm processing [17]. However, the SVM is

renowned for its capability to yield accurate outcomes, even when faced with a sparse training dataset. This can be attributed to its underlying principle, which suggests that only training samples at class boundaries are pivotal for a sharp distinction [89]. Nonetheless, a potential pitfall should be acknowledged: the SVM tends to falter in accuracy when the feature count surpasses the count of the training samples [90].

Neural networks, particularly ANNs, have gained prominence in RS for an extended period. ANNs are characterized by their dense structures, which are composed of interconnected neurons arranged in layers with specific weights assigned to these connections [19]. Notably, this algorithm has the advantage of navigating the mixed pixel challenge. However, it bears the burden of being notably time-intensive, especially when the node count increases [20]. Meanwhile, for the KNN algorithm, the K value emerged as a pivotal determinant of classifier efficacy. A low K value sketches a rudimentary decision boundary, whereas an elevated K value may usher in over-fitting and resultant model instability [19]. For practitioners, the silver lining lies in the feasibility of pinpointing the optimal K value for specific scenarios by iterative algorithm runs with varied K values, and subsequently selecting the best fitting one.

Lately, the ascendancy of XGBoost in the ML spectrum has been unmissable. Recognized for its advantages in both regression and classification, XGBoost slashes processing durations, prunes trees to deter overfitting, and leverages a block design for parallel computations [91,92]. Consequently, RF may find itself contending with XGBoost's burgeoning capabilities in foreseeable advancements.

The algorithmic precision of the RS data classification depends significantly on suitable parameter configurations [93]. Importantly, the perfect calibration for input parameters is a dynamic aspect, influenced by the class count and their intricacy. The care dedicated to the parameter settings directly echoes the classification results. In conclusion, the myriad elements influencing the classification process must be appreciated beyond data and algorithmic choices. The accuracy of statistical outputs can be contingent on facets such as the characteristics of the study locale, adopted classification framework, pixel granularity, and reference data integrity [94].

In this study, we conducted the first attempt to map LULC using a variety of ML classification methods and examined temporal changes over 30 years in Northeast Erbil Province. We employed five different MLAs to achieve high-accuracy assessments for the SVM, RF, ANN, KNN, and XGBoost algorithms, with overall accuracies of 93%–96 %, 94%–97.5 %, 92%–97 %, 93%–96.5 %, and 93%–96 %, respectively. The corresponding Kc were 0.91–0.95, 0.93–0.97, 0.91–0.96, 0.92–0.96, and 0.92–0.95, respectively. Notably, the Kc obtained for the classified images were all $>$0.9, indicating a high level of accuracy of the generated classified maps.

Furthermore, the effectiveness of the RF algorithm for LULC classification was supported by Khan and Sudheer [95]. They applied the RF algorithm to three decades of Landsat satellite imagery and achieved a high Kc of 0.93–0.97. This finding was consistent with the results of the present study. Adugna et al. [96] found that RF outperformed SVM, producing a Kc of 0.83, which was 3 % higher than that of SVM. Similarly, Ge et al. [20] obtained a higher Kc 0.96 for both RF and ANN and highlighted RF as the most effective classifier owing to its stability, user-friendliness, and processing speed during parameter tuning.

However, our study's findings differed from those of Abdi [42], who examined SVM, XGBoost, RF, and deep learning and reported overall accuracies of 75.8 %, 75.1 %, 73.9 %, and 73.3 %, respectively. This difference can be attributed to the use of Sentinel-2 data and seasonal analyses instead of annual data. Additionally, according to Al-Dousari et al. [97], the RF algorithm recorded a very high accuracy for LULC maps, with Kc of 0.86 and 0.93 for the years 2016 and 2021, respectively. They utilized high-resolution multi--temporal Sentinel imagery to derive LULC maps.

To implement future conservation measures effectively, a comprehensive understanding of the spatiotemporal land cover state of the Region is necessary [4]. In this study, multi-temporal TM and OLI Landsat images were used to differentiate LULC types in a large study area. Change detection analysis was then applied over a three-decade period, from 1991 to 2021. The analysis revealed significant shifts in land cover types between the two periods.

Several changes were observed during the first decade (1991–2001). Agricultural land and forest cover increased by 19 % and 7.9 %, respectively, whereas built-up areas improved by 0.27 %. However, this was accompanied by a 26.34 % degradation of rangelands and a 1.26 % increase in barren land. These changes were influenced by various interconnected factors, with political development, population growth, and socioeconomic concerns being the primary drivers [98]. This finding is consistent with that of Hamad et al. [28], who identified socioeconomic conditions resulting from the United Nations' post-war economic sanctions from 1991 to 2003 as the primary drivers of such shifts. Additionally, the encroachment of rangelands by villagers and suburban populations has contributed to these changes. This observation aligns with the findings of Khwarahm et al. [30] in Erbil Province, where unstable economic and political conditions were noted.

In the subsequent decade (2001–2010), changes in most LULC classes showed a trend reversal. Agricultural and forest land cover decreased by 7.96 % and 5.77 %, respectively, whereas rangeland and barren land increased by 10.46 % and 3.09 %, respectively. The decline in agricultural land and forest cover can be attributed to the rapid socioeconomic growth following the Fall of Baghdad. Moreover, an increase in forest fires, often resulting from shifts in land use and conflicts, has led to significant annual losses in forested areas [99]. Local villagers residing near forested areas have also contributed to deforestation by cutting trees along major upland roads for charcoal and firewood [31].

In the third and final decade, from 2010 to 2021, improvements were observed in rangeland (4.55 %), agricultural land (2.41 %), forest cover (1.3 %), riparian zones (0.42 %), and built-up areas (0.24 %). Conversely, barren land experienced the highest decrease of 8.51 %, while water bodies declined by 0.38 %, and snow cover by 0.03 %. These positive changes in rangeland, agricultural land, and forest cover indicated an overall increase in vegetation cover. The decrease in water bodies can be attributed to drought conditions, whereas the increase in riparian zones was the result of plantation efforts. Evaluating changes in LULC is crucial for understanding the intricate relationship between human activities and the natural environment. Fortunately, in the selected study area, these changes have led to significant improvements in the natural environment, owing to recent economic growth and political stability.

Although a relatively high classification accuracy was achieved, this study still has some limitations. The study area encompassed a large region with heterogeneous medium-resolution image classes, resulting in some mixing among classes, particularly in forest cover and other classes such as riparian forestry and water bodies. Additionally, the input datasets were not examined using deep learning algorithms, which could potentially enhance the accuracy. Xie and Niculescu [100] found that integrating convolutional neural networks with MLAs improved the classification performance by 5–10 % compared with other MLAs.

6. Conclusions

In this study, a comprehensive spatiotemporal analysis of LULC classification was conducted in a large area northeast of Erbil Province in the Kurdistan Region from 1991 to 2021. By incorporating elevation and NDVI layers alongside Landsat bands in a supervised classification system using five MLAs in the R environment, the following conclusions were drawn.

- All algorithms achieved notable accuracies, surpassing 92 %.
- The RF algorithm outperformed the other algorithms, exhibiting the highest accuracy with Kc values ranging from 0.93 to 0.97, followed by KNN, ANN, XGBoost, and SVM.
- Over the three-decade study period, the region experienced significant LULC changes, characterized by considerable expansions in agricultural land, built-up areas, forests, and riparian zones, and notable reductions in rangeland and barren land. Population displacement, political instability, and socioeconomic development played substantial roles in LULC transitions.
- The change detection analysis revealed a 13.54 % increase in agricultural land use and a 0.71 % increase in built-up areas, contributing to an 11.33 % decline in rangelands and a 6.68 % decrease in barren land. Additionally, forested areas had a positive growth rate of 3.43 % and riparian zones increased by 0.32 %.

These findings highlight expansion trends in agriculture, forestation, and urban development in the region. To manage these changes sustainably, local authorities should implement regulations for forest conservation and land use planning. The mountainous topography and moderate climate of the region also provide opportunities for economic investments in tourism. To further enhance the accuracy of the LULC classification, highly detailed aerial photography is recommended to obtain more precise reference data. Moreover, future research should explore the use of deep learning algorithms to achieve more accurate outcomes. These advancements will contribute to a better understanding and management of LULC changes, and guide decision-making processes for sustainable development and environmental preservation in the region.

Data availability statement

Data will be made available on request.

CRediT authorship contribution statement

Abdulqadeer Rash: Writing – review & editing, Writing – original draft, Methodology. **Yaseen Mustafa:** Supervision, Resources. **Rahel Hamad:** Supervision, Resources.

Declaration of competing interest

The authors declare that they have no known competing financial interests or personal relationships that could have appeared to influence the work reported in this paper.

Appendix A. Supplementary data

Supplementary data to this article can be found online at https://doi.org/10.1016/j.heliyon.2023.e21253.

References

[1] M.S. Mondal, N. Sharma, P.K. Garg, M. Kappas, Statistical independence test and validation of CA Markov land use land cover (LULC) prediction results, The Egyptian Journal of Remote Sensing and Space Science 19 (2016) 259–272.
[2] G. Vivekananda, R. Swathi, A. Sujith, Multi-temporal image analysis for LULC classification and change detection, European journal of remote sensing 54 (2021) 189–199.
[3] K. Islam, M. Jashimuddin, B. Nath, T.K. Nath, Land use classification and change detection by using multi-temporal remotely sensed imagery: the case of Chunati wildlife sanctuary, Bangladesh, The Egyptian Journal of Remote Sensing and Space Science 21 (2018) 37–47.
[4] G.T. Ayele, A.K. Tebeje, S.S. Demissie, M.A. Belete, M.A. Jemberrie, W.M. Teshome, D.T. Mengistu, E.Z. Teshale, Time series land cover mapping and change detection analysis using geographic information system and remote sensing, Northern Ethiopia, Air Soil. Water Res. 11 (2018), 1178622117751603.
[5] G. Fikadu, G. Olika, Impact of land use land cover change using remote sensing with integration of socio-economic data on Rural Livelihoods in the Nashe watershed, Ethiopia, Heliyon 9 (2023).
[6] C. Duhamel, Land use, Land cover, including their classification, Encylopedia of life support system 1 (2012) 1–9.

[7] S.K. Patel, P. Verma, G. Shankar Singh, Agricultural growth and land use land cover change in peri-urban India, Environ. Monit. Assess. 191 (2019) 1–17.
[8] Y. Sreedhar, A. Nagaraju, G.M. Krishna, An appraisal of land use/land cover change scenario of tummalapalle, cuddapah region, India—a remote sensing and GIS perspective, Adv. Rem. Sens. 5 (2016) 232–245.
[9] C. He, J. Zhang, Z. Liu, Q. Huang, Characteristics and progress of land use/cover change research during 1990–2018, J. Geogr. Sci. 32 (2022) 537–559.
[10] J. Rawat, M. Kumar, Monitoring land use/cover change using remote sensing and GIS techniques: a case study of Hawalbagh block, district Almora, Uttarakhand, India, The Egyptian Journal of Remote Sensing and Space Science 18 (2015) 77–84.
[11] S. Arshad, J. Hasan Kazmi, M. Fatima, N. Khan, Change detection of land cover/land use dynamics in arid region of Bahawalpur District, Pakistan, Applied Geomatics 14 (2022) 387–403.
[12] C. Liu, W. Li, G. Zhu, H. Zhou, H. Yan, P. Xue, Land use/land cover changes and their driving factors in the Northeastern Tibetan Plateau based on Geographical Detectors and Google Earth Engine: a case study in Gannan Prefecture, Rem. Sens. 12 (2020) 3139.
[13] E.L. Bullock, S.P. Healey, Z. Yang, P. Oduor, N. Gorelick, S. Omondi, E. Ouko, W.B. Cohen, Three decades of land cover change in East Africa, Land 10 (2021) 150.
[14] M. Schaefer, N.X. Thinh, Evaluation of Land Cover Change and Agricultural Protection Sites: A GIS and Remote Sensing Approach for Ho Chi Minh City, Vietnam. Heliyon *5*, 2019.
[15] R. Nedd, K. Light, M. Owens, N. James, E. Johnson, A. Anandhi, A synthesis of land use/land cover studies: definitions, classification systems, meta-studies, challenges and knowledge gaps on a global landscape, Land 10 (2021) 994.
[16] P.K. Mishra, A. Rai, S.C. Rai, Land use and land cover change detection using geospatial techniques in the Sikkim Himalaya, India, The Egyptian Journal of Remote Sensing and Space Science 23 (2020) 133–143.
[17] E. Adam, O. Mutanga, J. Odindi, E.M. Abdel-Rahman, Land-use/cover classification in a heterogeneous coastal landscape using RapidEye imagery: evaluating the performance of random forest and support vector machines classifiers, Int. J. Rem. Sens. 35 (2014) 3440–3458.
[18] P. Thanh Noi, M. Kappas, Comparison of random forest, k-nearest neighbor, and support vector machine classifiers for land cover classification using Sentinel-2 imagery, Sensors 18 (2017) 18.
[19] A.E. Maxwell, T.A. Warner, F. Fang, Implementation of machine-learning classification in remote sensing: an applied review, Int. J. Rem. Sens. 39 (2018) 2784–2817.
[20] G. Ge, Z. Shi, Y. Zhu, X. Yang, Y. Hao, Land use/cover classification in an arid desert-oasis mosaic landscape of China using remote sensed imagery: performance assessment of four machine learning algorithms, Global Ecology and Conservation 22 (2020), e00971.
[21] L. Ghayour, A. Neshat, S. Paryani, H. Shahabi, A. Shirzadi, W. Chen, N. Al-Ansari, M. Geertsema, M. Pourmehdi Amiri, M. Gholamnia, Performance evaluation of sentinel-2 and landsat 8 OLI data for land cover/use classification using a comparison between machine learning algorithms, Rem. Sens. 13 (2021) 1349.
[22] S. Amini, M. Saber, H. Rabiei-Dastjerdi, S. Homayouni, Urban land use and land cover change analysis using random forest classification of landsat time series, Rem. Sens. 14 (2022) 2654.
[23] A. Tariq, Y. Jiango, Q. Li, J. Gao, L. Lu, W. Soufan, K.F. Almutairi, M. Habib-ur-Rahman, Modelling, mapping and monitoring of forest cover changes, using support vector machine, kernel logistic regression and naive bayes tree models with optical remote sensing data, Heliyon 9 (2023).
[24] J. Liang, C. Chen, Y. Song, W. Sun, G. Yang, Long-term mapping of land use and cover changes using Landsat images on the Google Earth Engine Cloud Platform in bay area-A case study of Hangzhou Bay, China, Sustainable Horizons 7 (2023), 100061.
[25] S. Georganos, T. Grippa, S. Vanhuysse, M. Lennert, M. Shimoni, E. Wolff, Very high resolution object-based land use–land cover urban classification using extreme gradient boosting, Geosci. Rem. Sens. Lett. IEEE 15 (2018) 607–611.
[26] R. Hamad, H. Balzter, K. Kolo, Multi-criteria assessment of land cover dynamic changes in halgurd sakran national park (HSNP), kurdistan region of Iraq, using remote sensing and GIS, Land 6 (2017) 18.
[27] A. Al-Hameedawi, M. Buchroithner, Object-oriented Classifications for Land Use/land Cover Using Cosmo-SkyMed and LandSat 7 Satellite Data: an Example of Erbil/Iraq, VDE, 2014, pp. 1–4.
[28] R. Hamad, K. Kolo, H. Balzter, Post-war land cover changes and fragmentation in halgurd sakran national park (HSNP), kurdistan region of Iraq, Land 7 (2018) 38.
[29] M.S. Mohammad, N. Elmastas, H. Abdullah, Temporal change of urban land use: the case of Erbil city, Ecology, Environment and Conservation Paper 27 (2021) 48–58.
[30] N.R. Khwarahm, S. Qader, K. Ararat, A.M. Fadhil Al-Quraishi, Predicting and mapping land cover/land use changes in Erbil/Iraq using CA-Markov synergy model, Earth science informatics 14 (2021) 393–406.
[31] F.K. Bishay, Towards Sustainable Agricultural Development in Iraq. The Transition from Relief, Rehabilitation and Reconstruction to Development, 2003. https://www.fao.org/3/Y9870E/y9870e00.htm#Contents.
[32] H.E. Beck, N.E. Zimmermann, T.R. McVicar, N. Vergopolan, A. Berg, E.F. Wood, Present and future Köppen-Geiger climate classification maps at 1-km resolution, Sci. Data 5 (2018) 1–12.
[33] UNFPA, The Demographic Survey of the Kurdistan Region of Iraq, 2018. https://iraq.unfpa.org/en/publications/demographic-survey-kurdistan-region-iraq.
[34] KRSO, Kurdistan region of Iraq - population analysis report. https://krso.gov.krd/en, 2021.
[35] A. Eiumnoh, R.P. Shrestha, Application of DEM data to Landsat image classification: evaluation in a tropical wet-dry landscape of Thailand, Photogramm. Eng. Rem. Sens. 66 (2000) 297–304.
[36] N.E. Young, R.S. Anderson, S.M. Chignell, A.G. Vorster, R. Lawrence, P.H. Evangelista, A survival guide to Landsat preprocessing, Ecology 98 (2017) 920–932.
[37] T. Cooley, G.P. Anderson, G.W. Felde, M.L. Hoke, A.J. Ratkowski, J.H. Chetwynd, J.A. Gardner, S.M. Adler-Golden, M.W. Matthew, A. Berk, FLAASH, a MODTRAN4-Based Atmospheric Correction Algorithm, its Application and Validation, IEEE, 2002, pp. 1414–1418.
[38] J.R. Anderson, A Land Use and Land Cover Classification System for Use with Remote Sensor Data, US Government Printing Office, 1976.
[39] D. Lu, Q. Weng, A survey of image classification methods and techniques for improving classification performance, Int. J. Rem. Sens. 28 (2007) 823–870.
[40] R Core Team, R: A Language and Environment for Statistical Computing, 2022. https://www.R-project.org/.
[41] R.R. Rudra, S.K. Sarkar, Artificial neural network for flood susceptibility mapping in Bangladesh, Heliyon 9 (2023).
[42] A.M. Abdi, Land cover and land use classification performance of machine learning algorithms in a boreal landscape using Sentinel-2 data, GIScience Remote Sens. 57 (2020) 1–20.
[43] Y. Piao, S. Jeong, S. Park, D. Lee, Analysis of land use and land cover change using time-series data and random forest in North Korea, Rem. Sens. 13 (2021) 3501.
[44] G. Mountrakis, J. Im, C. Ogole, Support vector machines in remote sensing: a review, ISPRS J. Photogrammetry Remote Sens. 66 (2011) 247–259.
[45] V. Vapnik, Support-vector networks, Mach. Learn. 20 (1995) 273–297.
[46] P. Mantero, G. Moser, S.B. Serpico, Partially supervised classification of remote sensing images through SVM-based probability density estimation, IEEE Trans. Geosci. Rem. Sens. 43 (2005) 559–570.
[47] T. Kavzoglu, I. Colkesen, A kernel functions analysis for support vector machines for land cover classification, Int. J. Appl. Earth Obs. Geoinf. 11 (2009) 352–359.
[48] G. Guo, H. Wang, D. Bell, Y. Bi, K. Greer, KNN Model-Based Approach in Classification, Springer, 2003, pp. 986–996.
[49] Q. Meng, C.J. Cieszewski, M. Madden, B.E. Borders, K nearest neighbor method for forest inventory using remote sensing data, GIScience Remote Sens. 44 (2007) 149–165.
[50] E. Blanzieri, F. Melgani, Nearest neighbor classification of remote sensing images with the maximal margin principle, IEEE Trans. Geosci. Rem. Sens. 46 (2008) 1804–1811.
[51] G. Chirici, M. Mura, D. McInerney, N. Py, E.O. Tomppo, L.T. Waser, D. Travaglini, R.E. McRoberts, A meta-analysis and review of the literature on the k-Nearest Neighbors technique for forestry applications that use remotely sensed data, Rem. Sens. Environ. 176 (2016) 282–294.
[52] D.M. Miller, E.J. Kaminsky, S. Rana, Neural network classification of remote-sensing data, Comput. Geosci. 21 (1995) 377–386.

[53] P.M. Atkinson, A.R. Tatnall, Introduction neural networks in remote sensing, Int. J. Rem. Sens. 18 (1997) 699–709.
[54] L. Fausett, Fundamentals of Neural Networks: Architectures, Algorithms, and Applications, Prentice-Hall, Inc., 1994.
[55] S.B. Kotsiantis, I. Zaharakis, P. Pintelas, Supervised machine learning: a review of classification techniques, Emerging artificial intelligence applications in computer engineering 160 (2007) 3–24.
[56] J.F. Mas, J.J. Flores, The application of artificial neural networks to the analysis of remotely sensed data, Int. J. Rem. Sens. 29 (2008) 617–663.
[57] R.R. Jensen, P.J. Hardin, G. Yu, Artificial neural networks and remote sensing, Geography Compass 3 (2009) 630–646.
[58] S.A. Woznicki, J. Baynes, S. Panlasigui, M. Mehaffey, A. Neale, Development of a spatially complete floodplain map of the conterminous United States using random forest, Science of the total environment 647 (2019) 942–953.
[59] J. Corcoran, J. Knight, K. Pelletier, L. Rampi, Y. Wang, The effects of point or polygon based training data on RandomForest classification accuracy of wetlands, Rem. Sens. 7 (2015) 4002–4025.
[60] L. Breiman, Random forests, Mach. Learn. 45 (2001) 5–32.
[61] N. Horning, Random Forests: an Algorithm for Image Classification and Generation of Continuous Fields Data Sets, 2010, pp. 1–6.
[62] V.F. Rodriguez-Galiano, B. Ghimire, J. Rogan, M. Chica-Olmo, J.P. Rigol-Sanchez, An assessment of the effectiveness of a random forest classifier for land-cover classification, ISPRS J. Photogrammetry Remote Sens. 67 (2012) 93–104.
[63] T. Chen, C. Guestrin, Xgboost: A Scalable Tree Boosting System, 2016, pp. 785–794.
[64] Q.-T. Bui, T.-Y. Chou, T.-V. Hoang, Y.-M. Fang, C.-Y. Mu, P.-H. Huang, V.-D. Pham, Q.-H. Nguyen, D.T.N. Anh, V.-M. Pham, Gradient boosting machine and object-based CNN for land cover classification, Rem. Sens. 13 (2021) 2709.
[65] R.G. Congalton, K. Green, Assessing the Accuracy of Remotely Sensed Data: Principles and Practices, CRC press, 2019.
[66] M. Chowdhury, M.E. Hasan, M. Abdullah-Al-Mamun, Land use/land cover change assessment of Halda watershed using remote sensing and GIS, The Egyptian Journal of Remote Sensing and Space Science 23 (2020) 63–75.
[67] M.B. Lyons, D.A. Keith, S.R. Phinn, T.J. Mason, J. Elith, A comparison of resampling methods for remote sensing classification and accuracy assessment, Rem. Sens. Environ. 208 (2018) 145–153.
[68] R.G. Congalton, A review of assessing the accuracy of classifications of remotely sensed data, Rem. Sens. Environ. 37 (1991) 35–46.
[69] J.R. Jensen, Introductory Digital Image Processing: A Remote Sensing Perspective, Prentice Hall Press, 2015.
[70] C. Wu, B. Du, X. Cui, L. Zhang, A post-classification change detection method based on iterative slow feature analysis and Bayesian soft fusion, Rem. Sens. Environ. 199 (2017) 241–255.
[71] C. Chen, J. Liang, F. Xie, Z. Hu, W. Sun, G. Yang, J. Yu, L. Chen, L. Wang, L. Wang, Temporal and spatial variation of coastline using remote sensing images for Zhoushan archipelago, China, Int. J. Appl. Earth Obs. Geoinf. 107 (2022), 102711.
[72] A. Capolupo, C. Monterisi, M. Saponaro, E. Tarantino, Multi-temporal Analysis of Land Cover Changes Using Landsat Data through Google Earth Engine Platform, SPIE, 2020, pp. 447–458.
[73] M.M. El-Hattab, Applying post classification change detection technique to monitor an Egyptian coastal zone (Abu Qir Bay), The Egyptian Journal of Remote Sensing and Space Science 19 (2016) 23–36.
[74] J.S. Alawamy, S.K. Balasundram, C.T. Boon Sung, Detecting and analyzing land use and land cover changes in the region of Al-Jabal Al-Akhdar, Libya using time-series landsat data from 1985 to 2017, Sustainability 12 (2020) 4490.
[75] Y. Afaq, A. Manocha, Analysis on change detection techniques for remote sensing applications: a review, Ecol. Inf. 63 (2021), 101310.
[76] V.F. Rodriguez-Galiano, M. Chica-Rivas, Evaluation of different machine learning methods for land cover mapping of a Mediterranean area using multi-seasonal Landsat images and Digital Terrain Models, International Journal of Digital Earth 7 (2014) 492–509.
[77] J. Park, Y. Lee, J. Lee, Assessment of machine learning algorithms for land cover classification using remotely sensed data, Sensor. Mater. 33 (2021).
[78] A. Saha, M. Arora, E. Csaplovics, R. Gupta, Land cover classification using IRS LISS III image and DEM in a rugged terrain: a case study in Himalayas, Geocarto Int. 20 (2005) 33–40.
[79] L.B. Zeferino, L.F.T. de Souza, C.H. do Amaral, E.I. Fernandes Filho, T.S. de Oliveira, Does environmental data increase the accuracy of land use and land cover classification? Int. J. Appl. Earth Obs. Geoinf. 91 (2020), 102128.
[80] T.N. Phan, V. Kuch, L.W. Lehnert, Land cover classification using Google Earth Engine and random forest classifier—the role of image composition, Rem. Sens. 12 (2020) 2411.
[81] Z. Yu, L. Di, R. Yang, J. Tang, L. Lin, C. Zhang, M.S. Rahman, H. Zhao, J. Gaigalas, E.G. Yu, Selection of Landsat 8 OLI Band Combinations for Land Use and Land Cover Classification, IEEE, 2019, pp. 1–5.
[82] S. Tian, X. Zhang, J. Tian, Q. Sun, Random forest classification of wetland landcovers from multi-sensor data in the arid region of Xinjiang, China, Rem. Sens. 8 (2016) 954.
[83] K.M. Meingast, M.J. Falkowski, E.S. Kane, L.R. Potvin, B.W. Benscoter, A.M. Smith, L.L. Bourgeau-Chavez, M.E. Miller, Spectral detection of near-surface moisture content and water-table position in northern peatland ecosystems, Rem. Sens. Environ. 152 (2014) 536–546.
[84] Y.-Y. Chen, W. Huang, W.-H. Wang, J.-Y. Juang, J.-S. Hong, T. Kato, S. Luyssaert, Reconstructing Taiwan's land cover changes between 1904 and 2015 from historical maps and satellite images, Sci. Rep. 9 (2019) 3643.
[85] S.S. Aljenaid, G.R. Kadhem, M.F. AlKhuzaei, J.B. Alam, Detecting and assessing the spatio-temporal land use land cover changes of Bahrain Island during 1986–2020 using remote sensing and GIS, Earth Systems and Environment 6 (2022) 787–802.
[86] J. Li, Y. Zhou, Q. Li, S. Yi, L. Peng, Exploring the effects of land use changes on the landscape pattern and soil erosion of western Hubei province from 2000 to 2020, Int. J. Environ. Res. Publ. Health 19 (2022) 1571.
[87] K.N. Loukika, V.R. Keesara, V. Sridhar, Analysis of land use and land cover using machine learning algorithms on google earth engine for Munneru River Basin, India, Sustainability 13 (2021), 13758.
[88] I. Atef, W. Ahmed, R.H. Abdel-Maguid, Modelling of land use land cover changes using machine learning and GIS techniques: a case study in El-Fayoum Governorate, Egypt, Environ. Monit. Assess. 195 (2023) 637.
[89] C. Huang, L. Davis, J. Townshend, An assessment of support vector machines for land cover classification, Int. J. Rem. Sens. 23 (2002) 725–749.
[90] F. Melgani, L. Bruzzone, Classification of hyperspectral remote sensing images with support vector machines, IEEE Trans. Geosci. Rem. Sens. 42 (2004) 1778–1790.
[91] L. Zhong, L. Hu, H. Zhou, Deep learning based multi-temporal crop classification, Rem. Sens. Environ. 221 (2019) 430–443.
[92] O.F. AlThuwaynee, S.-W. Kim, M.A. Najemaden, A. Aydda, A.-L. Balogun, M.M. Fayyadh, H.-J. Park, Demystifying uncertainty in PM10 susceptibility mapping using variable drop-off in extreme-gradient boosting (XGB) and random forest (RF) algorithms, Environ. Sci. Pollut. Control Ser. 28 (2021) 43544–43566.
[93] H. Jafarzadeh, M. Mahdianpari, E. Gill, F. Mohammadimanesh, S. Homayouni, Bagging and boosting ensemble classifiers for classification of multispectral, hyperspectral and PolSAR data: a comparative evaluation, Rem. Sens. 13 (2021) 4405.
[94] Y. Shao, R.S. Lunetta, Comparison of support vector machine, neural network, and CART algorithms for the land-cover classification using limited training data points, ISPRS J. Photogrammetry Remote Sens. 70 (2012) 78–87.
[95] A. Khan, M. Sudheer, Machine learning-based monitoring and modeling for spatio-temporal urban growth of Islamabad, The Egyptian Journal of Remote Sensing and Space Science 25 (2022) 541–550.
[96] T. Adugna, W. Xu, J. Fan, Comparison of random forest and support vector machine classifiers for regional land cover mapping using coarse resolution FY-3C images, Rem. Sens. 14 (2022) 574.
[97] A.E. Al-Dousari, A. Mishra, S. Singh, Land use land cover change detection and urban sprawl prediction for Kuwait metropolitan region, using multi-layer perceptron neural networks (MLPNN), The Egyptian Journal of Remote Sensing and Space Science 26 (2023) 381–392.

[98] R. Hamad, A remote sensing and GIS-based analysis of urban sprawl in Soran District, Iraqi Kurdistan, SN Appl. Sci. 2 (2020) 1–9.
[99] FAO, Forests and Climate Change Working Paper 9, 2010. https://www.fao.org/forestry/24646-0acdf8232cda6c92cb3e7b460f00fbea.pdf.
[100] G. Xie, S. Niculescu, Mapping and monitoring of land cover/land use (LCLU) changes in the crozon peninsula (Brittany, France) from 2007 to 2018 by machine learning algorithms (support vector machine, random forest, and convolutional neural network) and by post-classification comparison (PCC), Rem. Sens. 13 (2021) 3899.